


Nonreciprocal photon blockade in cavity optomagnonics

Hong Xie ^{1,*} Le-Wei He,¹ Xiao Shang,^{2,3,4} Gong-Wei Lin,^{2,3,4} and Xiu-Min Lin^{2,3,4,†}

¹*Department of Mathematics and Physics, Fujian Jiangxia University, Fuzhou 350108, China*

²*Fujian Provincial Key Laboratory of Quantum Manipulation and New Energy Materials, College of Physics and Energy, Fujian Normal University, Fuzhou 350117, China*

³*Fujian Provincial Engineering Technology Research Center of Solar Energy Conversion and Energy Storage, Fuzhou 350117, China*

⁴*Fujian Provincial Collaborative Innovation Center for Advanced High-Field Superconducting Materials and Engineering, Fuzhou 350117, China*



(Received 21 May 2022; revised 23 August 2022; accepted 26 October 2022; published 7 November 2022)

We study nonreciprocal photon blockade in cavity optomagnonics, where a sphere of ferromagnetic crystal supports two optical whispering-gallery modes and one magnon mode. The interaction in cavity optomagnonics is subject to the selection rules involving conservation of angular momentum and energy, and the selection rules introduce a nonreciprocal coupling between linearly polarized photons and magnons. For given incident linearly polarized photons, the photon blockade occurs when the cavity is driven in one direction, but it disappears if the cavity is driven in the opposite direction. The results suggest that cavity optomagnonics could be a promising platform for studying chiral quantum optics and topological photonics.

DOI: [10.1103/PhysRevA.106.053707](https://doi.org/10.1103/PhysRevA.106.053707)

I. INTRODUCTION

For nonreciprocal devices, light transmission between any two points in space is different for opposite propagation directions. This mechanism has a wide range of applications in information processing and has become fundamental in photonic systems [1,2]. Nonreciprocity has been pursued for a long time through Faraday rotation in magneto-optical materials, and recently, nonmagnetic nonreciprocal optical devices were proposed using various methods for the purpose of integration [3–16].

Different from the classical Faraday effect, which is related to the rotation of the polarization plane of light when it propagates along the magnetization direction, the emerging field of cavity optomagnonics is interesting in coupling light to the dynamical magnetization excitations and not to the magnetization itself [17–39]. The quanta of the dynamical magnetization excitations, called magnons, inherit the ability of single spins precessing and hence their chirality [40]. The chirality of magnons enables nonreciprocal coupling between magnons and microwave photons, which has been exploited to realize the nonreciprocal transmission of the microwave photon [41–44]. The chirality of magnons can also introduce a nonreciprocal interaction between magnons and whispering-gallery-mode (WGM) optical photons in cavity optomagnonics [45–47], and nonreciprocal Brillouin light scattering has been demonstrated in experiments [48,49]. Although the nonreciprocity has been discussed in regard to the cavity magnonics system, those studies mainly focus on the classical regime, i.e., the transmission properties of classical light.

Nonreciprocal photon blockade is a purely quantum effect [50] which analyzes the nonreciprocal statistic properties of the transmitted photons and is expected to play a key role in chiral quantum technologies and topological photonics. The blockade effect means that a photon excited in the cavity will prevent the exciting of the second one. Photon blockade can be realized in a nonlinear system by blocking the second photon with large detuning [51–53] or utilizing the destructive interference in the two-photon excitation state [54–56]. Nonreciprocal photon blockade was first predicted by using the Fizeau drag in a spinning optical Kerr resonator [50], where a splitting of the resonance frequencies of the counter-circulating modes was introduced. Subsequently, nonreciprocal photon blockades were also researched in a spinning resonator coupled to an auxiliary system [57–61], an optomechanical system with directional nonlinear interaction [62], and a linear-nonlinear optical molecule [63].

In this paper, we study the nonreciprocal photon blockade in cavity optomagnonics, where a ferromagnetic sphere supports both optical WGMs and magnetostatic modes. On the one hand, the interaction in cavity optomagnonics is intrinsically nonlinear, in which an incident linearly polarized photon in WGMs is scattered into an orthogonally polarized photon by eliminating or creating a magnon. On the other hand, the interaction is subject to selection rules involving the conservation of angular momentum and energy. Because the angular momenta of the WGM photons have opposite signs for counterclockwise (CCW) and clockwise (CW) circulations, the selection rules are different for the two circulations, leading to nonreciprocal optomagnonic coupling. We show that such nonlinear nonreciprocal optomagnonic coupling can be utilized for the realization of nonreciprocal photon blockade; that is, strong photon antibunching appears in a nonreciprocal way for the CCW or CW input.

*xh@fjxxu.edu.cn

†xmlin@fjnu.edu.cn

This paper is organized as follows. The model of optomagnonic interaction and nonreciprocity of the selection rules are studied in Sec. II. Nonreciprocal photon blockade is discussed by analyzing the statistic properties of CCW and CW photons in Sec. III. Finally, Sec. IV gives the conclusions.

II. NONRECIPROCAL OPTOMAGNONIC COUPLING

A. Optomagnonic interaction

Cavity optomagnonics is the study of the interaction of magnets with light. The starting point of studies is usually the dielectric tensor $\vec{\epsilon}(\mathbf{M})$ as a function of magnetization \mathbf{M} in the displacement field $\mathbf{D} = \vec{\epsilon}(\mathbf{M}) \cdot \mathbf{E}$. To the leading order of $\vec{\epsilon}$ in magnetization \mathbf{M} , the components of the permittivity tensor are [64]

$$\epsilon_{\alpha\beta}(\mathbf{M}) = \epsilon_0(\epsilon_r \delta_{\alpha\beta} - if \epsilon_{\alpha\beta\gamma} M_\gamma), \quad (1)$$

where ϵ_0 (ϵ_r) is the vacuum (relative) permittivity, $\delta_{\alpha\beta}$ represents the Kronecker delta function, and $\epsilon_{\alpha\beta\gamma}$ denotes the Levi-Civita tensor with spatial indices α , β , and γ . The second term on the right-hand side of Eq. (1) parameterizes the Faraday effect, and the constant f is related to the Faraday rotation coefficient, which can be obtained by experiments. Here, the second-order term of $\vec{\epsilon}$ in \mathbf{M} , called the Cotton-Mouton effect, has been disregarded since it is not essential for the configurations discussed in this paper.

For nondispersive media, the permittivity tensor is independent of frequency, and the average electromagnetic energy reads [36]

$$E_{\text{EM}} = \frac{1}{4} \int d\mathbf{r} \sum_{\alpha\beta} (\mathbf{E}_\alpha^* \epsilon_{\alpha\beta} \mathbf{E}_\beta + \mathbf{H}_\alpha^* \mu_{\alpha\beta} \mathbf{H}_\beta), \quad (2)$$

where \mathbf{E} (\mathbf{H}) expresses the electric (magnetic) field and $\mu_{\alpha\beta}$ indicates the permeability tensor. The permeability can be set to that of the vacuum at high optical frequencies, and the magneto-optical coupling is modeled through the dielectric permittivity tensor. The modification of the electromagnetic energy is introduced by the magnetization-dependent part of the permittivity, and the modification is given by

$$U_{\text{MO}} = -\frac{i}{4} \epsilon_0 f \int d\mathbf{r} \mathbf{M}(\mathbf{r}, t) \cdot [\mathbf{E}^*(\mathbf{r}, t) \times \mathbf{E}(\mathbf{r}, t)]. \quad (3)$$

The optomagnonic system is interesting in coupling light to the dynamics of the magnetization, not the magnetization itself. Thus, we describe the magnetization $\mathbf{M}(\mathbf{r}, t)$ by an excitation $\delta\mathbf{M}(\mathbf{r}, t)$ around the saturated magnetization \mathbf{M}_S , i.e., $\mathbf{M}(\mathbf{r}, t) = \mathbf{M}_S + \delta\mathbf{M}(\mathbf{r}, t)$. In the case of small deviations $|\delta\mathbf{M}| \ll |\mathbf{M}_S|$, the magnetization can be quantized as $\delta\mathbf{M}(\mathbf{r}, t) \rightarrow \frac{M_S}{2} \sum_\eta [\mathbf{w}_\eta(\mathbf{r}) \hat{m}_\eta + \mathbf{w}_\eta^*(\mathbf{r}) \hat{m}_\eta^\dagger]$, where \hat{m}_η is the annihilation operator of the magnon mode η and $\mathbf{w}_\eta(\mathbf{r})$ denotes the mode amplitude. The electric field of the light can also be quantized as $\mathbf{E}(\mathbf{r}, t) \rightarrow \sum [\mathbf{E}(\mathbf{r}) \hat{a} + \mathbf{E}^*(\mathbf{r}) \hat{a}^\dagger]$, with the mode function $\mathbf{E}(\mathbf{r})$ and the annihilation operator \hat{a} of the optical mode. The quantization procedure leads to the optomagnonic interaction Hamiltonian ($\hbar = 1$) [36,45]

$$\hat{H}_{\text{MO}} = \sum_{pq\eta} \hat{a}_p \hat{a}_q^\dagger (G_{pq\eta}^+ \hat{m}_\eta + G_{pq\eta}^- \hat{m}_\eta^\dagger) + \text{H.c.}, \quad (4)$$

where energy-nonconserving terms such as $\hat{a}_p^\dagger \hat{a}_q^\dagger \hat{m}_\eta$ have been discarded in the rotating-wave approximation and the static Faraday effect introduced by \mathbf{M}_S is ignored since it makes no contribution to the interaction. The couplings $G_{pq\eta}^+$ ($G_{pq\eta}^-$) parameterizes the anti-Stokes (Stokes) scattering amplitude of a photon from mode p to q by the annihilation (creation) of a magnon in mode η . The coupling constants are

$$G_{pq\eta}^+ = -\frac{i}{4} \epsilon_0 f \frac{M_S}{2} \int d\mathbf{r} \mathbf{w}_\eta(\mathbf{r}) \cdot [\mathbf{E}_p(\mathbf{r}) \times \mathbf{E}_q^*(\mathbf{r})], \quad (5a)$$

$$G_{pq\eta}^- = -\frac{i}{4} \epsilon_0 f \frac{M_S}{2} \int d\mathbf{r} \mathbf{w}_\eta^*(\mathbf{r}) \cdot [\mathbf{E}_p(\mathbf{r}) \times \mathbf{E}_q^*(\mathbf{r})]. \quad (5b)$$

The coupling can be determined when the normalizations of the optical and magnon modes are specified. The normalization of optical fields is obtain as $\int d\mathbf{r} |\mathbf{E}_p(\mathbf{r})|^2 = \hbar\omega_p/2\epsilon_0\epsilon_r$ with the frequency ω_p of mode p . We can then define $\mathbf{E}_p(\mathbf{r}) = \sqrt{\hbar\omega_p/2\epsilon_0\epsilon_r V_p} \mathbf{u}_p(\mathbf{r})$, where the mode function $\mathbf{u}_p(\mathbf{r})$ is normalized to the effective mode volume $\int d\mathbf{r} \mathbf{u}_p(\mathbf{r}) \cdot \mathbf{u}_p^*(\mathbf{r}) = V_p \delta_{p,p'}$ [36,37]. The effective mode volume V_p describes the spatial extension of the optical field, which is useful for dealing with optical surface states. For magnon modes, the normalization is expressed as $\int d\mathbf{r} |\mathbf{w}_\eta(\mathbf{r})|^2 = 4g_z \mu_B / M_S$, where g_z is the Landé factor and μ_B is the Bohr magneton [25,45]. It is physically appealing to adopt an effective magnon mode volume as in optics, $\int d\mathbf{r} \mathbf{w}_\eta(\mathbf{r}) \cdot \mathbf{v}_\eta^*(\mathbf{r}) = V_m \delta_{\eta,\eta'}$, and we have $\mathbf{w}_\eta(\mathbf{r}) = \sqrt{4g_z \mu_B / M_S V_m} \mathbf{v}_\eta(\mathbf{r})$. The effective mode volume V_m is a measure of the spatial extent of the magnon mode in the sample, which is valid for circularly polarized magnon modes.

The normalized coupling constant can be expressed as

$$G_{pq\eta}^+ = -\frac{i}{4} \epsilon_0 f \frac{M_S}{2} \sqrt{\frac{4g_z \mu_B}{M_S V_m} \frac{\omega}{2\epsilon_0 \epsilon_r V}} V_{\text{int}}^+, \quad (6a)$$

$$G_{pq\eta}^- = -\frac{i}{4} \epsilon_0 f \frac{M_S}{2} \sqrt{\frac{4g_z \mu_B}{M_S V_m} \frac{\omega}{2\epsilon_0 \epsilon_r V}} V_{\text{int}}^-, \quad (6b)$$

where

$$V_{\text{int}}^+ = \int d\mathbf{r} \mathbf{w}_\eta(\mathbf{r}) \cdot [\mathbf{u}_p(\mathbf{r}) \times \mathbf{u}_q^*(\mathbf{r})], \quad (7a)$$

$$V_{\text{int}}^- = \int d\mathbf{r} \mathbf{w}_\eta^*(\mathbf{r}) \cdot [\mathbf{u}_p(\mathbf{r}) \times \mathbf{u}_q^*(\mathbf{r})] \quad (7b)$$

are the overlap integrals of the three mode functions. Here, we have assumed that the optical mode frequencies and volumes differ slightly, i.e., $\omega_p \approx \omega_q \equiv \omega$ and $V_p \approx V_q \equiv V$. Note that small mode volumes and a large triple-mode overlap are required for large coupling.

B. Optical WGMs and magnetostatic modes in a ferromagnetic sphere

The expressions of coupling equations (5) and (6) are general and allow us to treat many configurations [22,65]. In this paper, we study the optomagnonic coupling in an yttrium iron garnet (YIG) sphere, which supports both magnetostatic modes and optical WGMs. YIG is currently the most often used material in cavity optomagnonics because of its

high Curie temperature and high optical and magnetic quality factors [37].

The optical modes in YIG sphere are specified by collective indices $\{l, m, n\}$, where the indices $(n - 1)$, $(l - m)$, and m are the numbers of radial, polar, and azimuthal nodes in the electric field [66], respectively. The optical WGMs are those modes which satisfy $l \gg 1$ and $m \approx \pm l$, where the sign of m corresponds to the light circulation direction; $m > 0$ ($m < 0$) refers to the CCW (CW) WGMs in the cavity.

The degeneracy of WGMs is broken at boundaries in favor of transverse electric (TE) and transverse magnetic (TM) modes, corresponding to a polarization in plane and out of plane with respect to the equator. The frequencies of TE and TM modes with the same indices are split by geometrical birefringence B_G with $B_G = R_{FS}\sqrt{1 - 1/n_r^2}$, where n_r is the refractive index of YIG and R_{FS} is the free spectral range [19]. For a millimeter-sized sphere, the results $R_{FS} \sim 40$ GHz and $B_G \sim 32$ GHz have been experimentally demonstrated [49].

The magnetostatic modes can be characterized by three indices $\{l_m, m_m, n_m\}$. The simplest magnetostatic mode is the nodeless uniform mode, namely, the Kittel mode, which is labeled $\{1_m, 1_m, 0_m\}$. The Kittel mode has zero orbital angular momentum, $-(m_m - 1) = 0$, and spin angular momentum $S_z = 1$ [37]. Thus, the total angular momentum of the Kittel mode is 1. A typical frequency of the Kittel mode is in the gigahertz range, which can be tuned by an external magnetic field close to $R_{FS} - B_G \sim 8$ GHz.

C. Selection rules

For incident linearly polarized photons, the expressions for V_{int}^{\pm} in Eq. (7) imply that the TE \rightarrow TE and TM \rightarrow TM scattering probabilities vanish, and the scattering with orthogonal polarizations TE \rightarrow TM and TM \rightarrow TE maximizes the coupling.

TE-CCW input. Consider TE-CCW incident WGMs $p = \{l, m, n, \text{TE}\}$ scattered into $q = \{l', m', n', \text{TM}\}$ by a Kittel mode $\{1_m, 1_m, 0_m\}$. The conservation of angular momentum is expected due to the axial symmetry of the system, and it can be revealed by the solutions of integrals V_{int}^{\pm} . Based on the orthonormality of the spherical harmonics, the integrals V_{int}^{\pm} can be calculated in polar coordinates, and the coupling strengths are given by [45]

$$G_{pq\eta, \text{ccw}}^{\pm} = g_{\pm} \delta_{n, n'} \delta_{m, m' \mp 1} \delta_{l, l' \mp 1}, \quad (8)$$

where $g_{\pm} = \pm \frac{\omega_f M_s}{8\epsilon_r} \sqrt{\frac{1}{sV_m}}$, with the spin number density $s = M_s/g_z \mu_B$. The coupling constants $G_{pq\eta, \text{ccw}}^{\pm}$ capture the selection rules of the optomagnonic interaction [23], which indicate the incident WGMs $p = \{l, m, n, \text{TE}\}$ can be scattered into only $q = \{l - 1, m - 1, n, \text{TM}\}$ in the Stokes scattering process with amplitude $G_{pq\eta, \text{ccw}}^{-}$ or $q = \{l + 1, m + 1, n, \text{TM}\}$ in the anti-Stokes scattering process with amplitude $G_{pq\eta, \text{ccw}}^{+}$.

The optical transitions for the CCW input are shown in Fig. 1(b). The amplitudes $G_{pq\eta, \text{ccw}}^{-}$ of the Stokes scattering $l \rightarrow l - 1$ are maximized when the magnon frequency ω_m is tuned to $R_{FS} - B_G$. However, the anti-Stokes transition $l \rightarrow l + 1$ is highly detuned by $R_{FS} + B_G + \omega_m \sim 80$ GHz, and hence, $G_{pq\eta, \text{ccw}}^{+} \approx 0$.

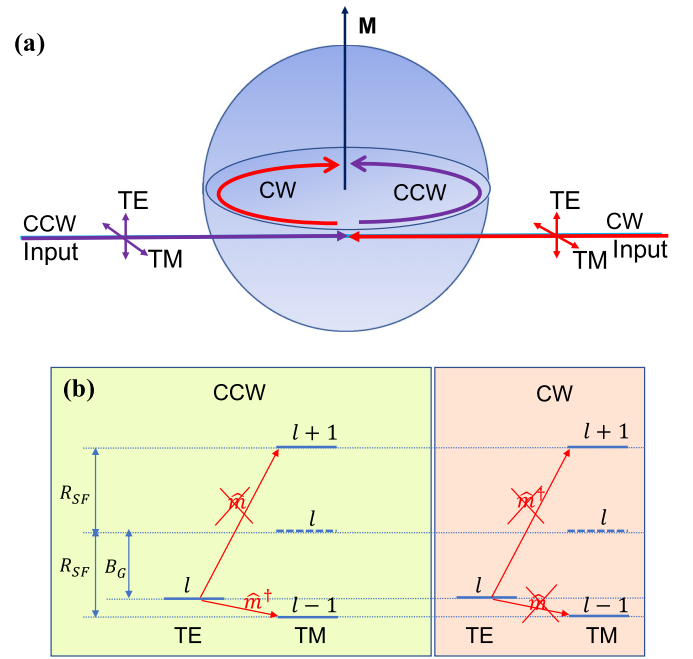


FIG. 1. (a) Schematic diagram of a cavity optomagnonic system. (b) Spectrum of the optical modes and schematic diagram of the selection rules in Eqs. (8) and (10). R_{SF} is the free spectral range, and B_G is the TM-TE splitting by geometrical birefringence. For a millimeter-sized YIG sphere, the typical magnon frequency ω_m can be tuned close to $R_{FS} - B_G$. For TE incident light, only the Stokes scattering in CCW mode associates with the transition $l \rightarrow l - 1$ is allowed, leading to nonreciprocal optomagnonic interaction.

In the scattering processes, the angular momentum of the Kittel mode is transferred between optical TE and TM modes, and the azimuthal mode index m of the WGMs must change by 1. When the magnon mode is tuned to the $\Delta m = -1$ transition, the $\Delta m = 1$ transition will be highly suppressed by the large detuning induced by the geometrical birefringence. This leads to an asymmetrical Brillouin light scattering, which was demonstrated in recent experiments [18,19,48].

Therefore, the interaction Hamiltonian (4) for the TE-CCW input can be reduced to

$$\hat{H}_{\text{int}}^{\text{ccw}} = G(\hat{a}_{\text{TE}} \hat{a}_{\text{TM}}^{\dagger} \hat{m}^{\dagger} + \hat{a}_{\text{TE}}^{\dagger} \hat{a}_{\text{TM}} \hat{m}), \quad (9)$$

where the coupling constant $G_{pq\eta, \text{ccw}}^{-}$ has been rewritten as G for simplicity. The interaction Hamiltonian indicates that the annihilation (creation) of a photon in the TE mode is accompanied by the creation (annihilation) of a magnon and a photon in the TM mode, and the frequencies of the three modes satisfy $\omega_{\text{TE}} = \omega_{\text{TM}} + \omega_m$.

TE-CW input. On the other hand, for the TE-CW incident WGMs, the sign of the azimuthal number of WGMs is $m < 0$. The coupling strength $G_{pq\eta, \text{cw}}^{\pm}$ can be calculated as

$$G_{pq\eta, \text{cw}}^{\pm} = g_{\pm} \delta_{n, n'} \delta_{m, m' \mp 1} \delta_{l, l' \pm 1}. \quad (10)$$

In this case, the incident WGMs $p = \{l, m, n, \text{TE}\}$ can be scattered into $q = \{l + 1, m - 1, n, \text{TM}\}$ in the Stokes scattering process with amplitude $G_{pq\eta, \text{cw}}^{-}$ or into $q = \{l - 1, m + 1, n, \text{TM}\}$ in the anti-Stokes scattering process with amplitude $G_{pq\eta, \text{cw}}^{+}$.

The Stokes scattering $l \rightarrow l + 1$ is accompanied by the creation of a magnon, and the angular momentum is transferred from WGMs to the Kittel mode, which is consistent with angular momentum conservation. However, the transition $l \rightarrow l + 1$ is detuned by $R_{\text{FS}} + B_{\text{G}} - \omega_m \sim 64$ GHz, as shown in Fig. 1(b). The anti-Stokes scattering $l \rightarrow l - 1$ occurs by annihilating a magnon, and the angular momentum of the Kittel mode is transferred to the TM mode. But the transition $l \rightarrow l - 1$ is also nonresonant with a detuning $R_{\text{FS}} - B_{\text{G}} + \omega_m \sim 16$ GHz, which is larger than the typical cavity linewidth $\kappa = 1$ GHz. Hence, both the Stokes and anti-Stokes scattering processes are highly suppressed, $G_{pqm, \text{cw}}^{\pm} \approx 0$, and the optomagnonic interaction is absent for the CW mode,

$$\hat{H}_{\text{int}}^{\text{cw}} = 0. \quad (11)$$

For incident TE-CW photons, the increase (reduction) in angular momentum of optical WGMs is accompanied by a reduction (increase) in the energy, which is not favorable for the transitions, leading to the absence of optomagnonic coupling.

As discussed above, the selection rules are different for CCW and CW inputs. This results in the nonreciprocal optomagnonic coupling, which has been demonstrated in experiments in terms of Brillouin light scattering [48,49]. The nonreciprocal characteristics of the selection rules can be understood by the chirality of optical WGMs. The angular momenta of optical WGMs have opposite signs for different circulation directions; the angular momentum $m > 0$ for the CCW mode, and $m < 0$ for the CW mode. In the scattering processes, the angular momentum is transferred between magnons and WGMs photons. When the light is input in the opposite circulation direction, the processes of magnon creation and annihilation, that is, the Stokes and anti-Stokes scattering processes, must be exchanged because of angular momentum conservation, leading to the nonreciprocal selection rules.

So far, the above discussions have focused on the TE incident photons. The results can be extended to the TM incident photons, and similar selection rules can be obtained [46,49]. In the following, we discuss only the case of TE incident WGMs for clarity.

III. NONRECIPROCAL PHOTON BLOCKADE

A. Anharmonic energy level in few-photon subspace

The Hamiltonian $\hat{H}_{\text{int}}^{\text{ccw}}$ in Eq. (9) presents a nonlinear optomagnonic coupling which enables a resonant interaction between states $|n_{\text{TE}}, n_{\text{TM}}, m_{\text{K}}\rangle$ and $|n_{\text{TE}} - 1, n_{\text{TM}} + 1, m_{\text{K}} + 1\rangle$ with amplitudes $G\sqrt{n_{\text{TE}}(n_{\text{TM}} + 1)(m_{\text{K}} + 1)}$, where n_{TE} , n_{TM} , and m_{K} denote the photon numbers of the TE mode and the TM mode and the magnon number of the Kittel mode, respectively. The nonlinear interaction is crucial to realize the photon blockade [67]. To show this more clearly, we diagonalize the Hamiltonian $\hat{H}_{\text{int}}^{\text{ccw}}$ in the few-photon subspace. In the zero-photon subspace, obviously, the eigenstate of the Hamiltonian is $|0_0\rangle = |000\rangle$, and the eigenvalue is zero. In the one-photon subspace $\{|100\rangle, |011\rangle\}$, the Hamiltonian can be expressed as

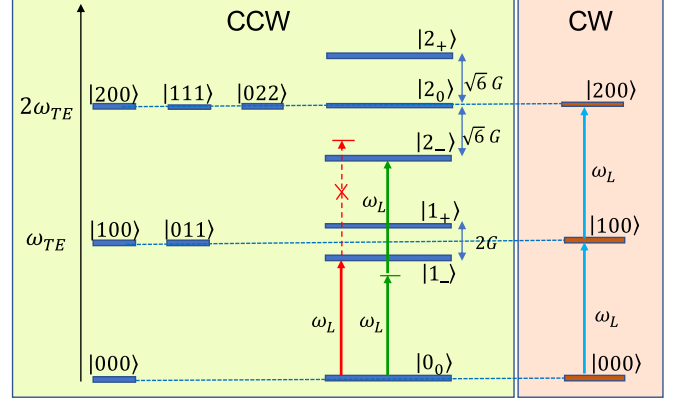


FIG. 2. Energy level of the system in the few-photon subspace. States are labeled $|n_{\text{TE}}, n_{\text{TM}}, m_{\text{K}}\rangle$, where n_{TE} and n_{TM} are the photon numbers of the TE and TM modes and m_{K} denotes the magnon number. Left: The optomagnonic coupling between the CCW optical mode and the Kittel mode splits the degeneracy of the states into the one- and two-photon subspaces, leading to an anharmonic energy level of the system. Red arrows denote the single-photon blockade; green arrows indicate the two-photon transition. Right: The CW optical mode which does not couple to Kittel mode presents a harmonic energy level.

a matrix with the form

$$\hat{H}_{\text{int}}^{\text{ccw}} = \begin{pmatrix} 0 & G \\ G & 0 \end{pmatrix}, \quad (12)$$

which can be diagonalized, resulting in the eigenstates $|1_{\pm}\rangle = \frac{1}{\sqrt{2}}(|100\rangle \pm |011\rangle)$ and the corresponding eigenvalues $\pm G$. The Hamiltonian has the form

$$\hat{H}_{\text{int}}^{\text{ccw}} = \begin{pmatrix} 0 & \sqrt{2}G & 0 \\ \sqrt{2}G & 0 & 2G \\ 0 & 2G & 0 \end{pmatrix} \quad (13)$$

in the two-photon subspace $\{|200\rangle, |111\rangle, |022\rangle\}$, and the eigenstates are $|2_0\rangle = \frac{1}{\sqrt{3}}(\sqrt{2}|200\rangle - |022\rangle)$ and $|2_{\pm}\rangle = \frac{1}{\sqrt{6}}(|200\rangle \pm \sqrt{3}(|111\rangle + \sqrt{2}|022\rangle))$, with eigenvalues of zero and $\pm\sqrt{6}G$, respectively.

The energy level of the system in the few-photon subspace is presented in the left panel of Fig. 2. Due to the nonlinear optomagnonic coupling in the CCW direction, the degeneracy of the states is split in the one-photon and two-photon subspaces, which gives rise to an anharmonic energy level of the system. The anharmonic energy level can be exploited to realize photon blockade, analogous to that implemented by using the Jaynes-Cummings ladder of the atom-cavity system [52,53].

Consider a weak field with frequency ω_L used to drive the TE-CCW mode. When the TE-CCW mode is driven at detuning $\Delta = \omega_{\text{TE}} - \omega_L = \pm G$, the single-photon resonance transitions $|0_0\rangle \rightarrow |1_{\pm}\rangle$ take place, and the subsequent transitions $|1_{\pm}\rangle \rightarrow |2_0\rangle, |2_{\pm}\rangle$ are suppressed for large detuning, leading to the single-photon blockade. For a CCW mode driven at $2\Delta = \pm\sqrt{6}G$, the two-photon transitions $|0_0\rangle \rightarrow |2_{\pm}\rangle$ dominate, which is often referred to two-photon blockade or photon-induced tunneling.

In contrast to the CCW mode, there is no coupling between the optical modes and the Kittel mode in the CW direction. Thus, the system presents a harmonic energy level, where the photon blockade never happens, as shown in the right panel of Fig. 2.

B. Second-order correlation function

The full Hamiltonian includes the free-evolution part, and the driving term reads

$$\hat{H} = \hat{H}_0 + \hat{H}_{\text{int}} + \hat{H}_{\text{dr}}, \quad (14)$$

where the interaction Hamiltonian \hat{H}_{int} is $\hat{H}_{\text{int}}^{\text{ccw}}$ for the CCW mode and $\hat{H}_{\text{int}}^{\text{cw}}$ for the CW mode. The free-evolution part of the system is

$$\hat{H}_0 = \omega_{\text{TE}} \hat{a}_{\text{TE}}^\dagger \hat{a}_{\text{TE}} + \omega_{\text{TM}} \hat{a}_{\text{TM}}^\dagger \hat{a}_{\text{TM}} + \omega_{\text{m}} \hat{m}^\dagger \hat{m}, \quad (15)$$

and the driving term

$$\hat{H}_{\text{dr}} = \Omega_L (\hat{a}_{\text{TE}} e^{i\omega_L t} + \hat{a}_{\text{TE}}^\dagger e^{-i\omega_L t}), \quad (16)$$

with the amplitude Ω_L of the driving field.

When the dissipations of optical modes and the Kittel mode are taken into account, the dynamical evolution of the system is described in terms of the density matrix ρ by the master equation

$$\begin{aligned} \dot{\rho} = & -i[\hat{H}, \rho] + \frac{\kappa}{2} \mathcal{D}(\hat{a}_{\text{TE}}) \rho + \frac{\kappa}{2} \mathcal{D}(\hat{a}_{\text{TM}}) \rho \\ & + \frac{\gamma}{2} \bar{n}_{\text{th}} \mathcal{D}(\hat{m}^\dagger) \rho + \frac{\gamma}{2} (\bar{n}_{\text{th}} + 1) \mathcal{D}(\hat{m}) \rho, \end{aligned} \quad (17)$$

where $\mathcal{D}(\hat{\delta})\rho = 2\hat{\delta}\rho\hat{\delta}^\dagger - \hat{\delta}^\dagger\hat{\delta}\rho - \rho\hat{\delta}^\dagger\hat{\delta}$, κ and γ are the decay rates of optical modes and the Kittel mode, respectively, and $\bar{n}_{\text{th}} = 1/[\exp(\hbar\omega_{\text{m}}/k_B T) - 1]$ denotes the thermal magnon number at the environmental temperature T .

The photon statistical properties of the optical CCW and CW modes can be characterized by the equal-time second-order correlation function

$$g^{(2)}(0) = \frac{\langle \hat{a}^{\dagger 2} \hat{a}^2 \rangle}{\langle \hat{a}^\dagger \hat{a} \rangle^2} = \frac{\text{Tr}(\hat{a}^{\dagger 2} \hat{a}^2 \rho_s)}{\text{Tr}(\hat{a}^\dagger \hat{a} \rho_s)^2}, \quad (18)$$

where ρ_s is the steady-state solution of the density matrix. It is known that the correlation function $g^{(2)}(0) < 1$ [$g^{(2)}(0) > 1$] corresponds to the photon antibunching (bunching) effect, and the limit $g^{(2)}(0) \rightarrow 0$ indicates the complete photon blockade in which only one photon can be excited in the optical mode [51–53].

To study the detailed conditions for photon blockade in the CCW mode, we calculate the correlation function approximately in a truncated Fock space. Assuming that the optomagnonic system is initially cooled to its ground state, when the TE-CCW mode is driven by a sufficiently weak driving field, only a few photons can be excited. Hence, the state of the system can be expanded in the few-photon subspace

$$\begin{aligned} |\psi(t)\rangle = & C_{000}|000\rangle + C_{100}|100\rangle + C_{011}|011\rangle \\ & + C_{200}|200\rangle + C_{111}|111\rangle + C_{022}|022\rangle, \end{aligned} \quad (19)$$

where the coefficients $C_{n_{\text{TE}}, n_{\text{TM}}, m_{\text{K}}}$ denote the probability amplitudes of the corresponding states. Then the second-order

correlation function of the TE-CCW mode can be written as

$$g_{\text{ccw}}^{(2)}(0) = \frac{2|C_{200}|^2}{(|C_{100}|^2 + |C_{111}|^2 + 2|C_{200}|^2)^2}. \quad (20)$$

In order to calculate the correlation function, the full Hamiltonian \hat{H} for the CCW mode is transformed into the frame defined by the unitary operator $U = e^{i(\hat{a}_{\text{TE}}^\dagger \hat{a}_{\text{TE}} + \hat{a}_{\text{TM}}^\dagger \hat{a}_{\text{TM}})\omega_L t}$ to make the driving term time independent. Thus, we have

$$\begin{aligned} \hat{H}^{\text{ccw}} = & \Delta \hat{a}_{\text{TE}}^\dagger \hat{a}_{\text{TE}} + (\Delta - \omega_{\text{m}}) \hat{a}_{\text{TM}}^\dagger \hat{a}_{\text{TM}} + \omega_{\text{m}} \hat{m}^\dagger \hat{m} \\ & + G(\hat{a}_{\text{TE}} \hat{a}_{\text{TM}}^\dagger \hat{m}^\dagger + \hat{a}_{\text{TE}}^\dagger \hat{a}_{\text{TM}} \hat{m}) + \Omega_L (\hat{a}_{\text{TE}} + \hat{a}_{\text{TE}}^\dagger). \end{aligned} \quad (21)$$

Consider an effective non-Hermitian Hamiltonian

$$\hat{H}_{\text{eff}} = \hat{H}^{\text{ccw}} - i\frac{\kappa}{2}(\hat{a}_{\text{TE}}^\dagger \hat{a}_{\text{TE}} + \hat{a}_{\text{TM}}^\dagger \hat{a}_{\text{TM}}) - i\frac{\gamma}{2}\hat{m}^\dagger \hat{m}, \quad (22)$$

and substitute it into the Schrödinger equation $id|\psi\rangle/dt = H_{\text{eff}}|\psi\rangle$; the probability amplitudes can be calculated by the following equations of motion:

$$i\dot{C}_{000} = \Omega_L C_{100}, \quad (23a)$$

$$i\dot{C}_{100} = \kappa' C_{100} + GC_{011} + \Omega_L C_{000} + \sqrt{2}\Omega_L C_{200}, \quad (23b)$$

$$i\dot{C}_{011} = \kappa' C_{011} + GC_{100} + \Omega_L C_{111}, \quad (23c)$$

$$i\dot{C}_{200} = 2\kappa' C_{200} + \sqrt{2}GC_{111} + \sqrt{2}\Omega_L C_{100}, \quad (23d)$$

$$i\dot{C}_{111} = 2\kappa' C_{111} + \sqrt{2}GC_{200} + 2GC_{022} + \Omega_L C_{011}, \quad (23e)$$

$$i\dot{C}_{022} = 2\kappa' C_{022} + 2GC_{111}, \quad (23f)$$

where $\kappa' = \Delta - i\kappa/2$ and we have neglected the magnon decay rate by assuming $\gamma \ll \kappa$. In the weak-driving regime $\Omega_L \ll \kappa$, only a few photons will be excited. In the limit $\Omega_L \rightarrow 0$, we have $C_{000} \rightarrow 1$, and the system approaches the ground state. Hence, the probability amplitudes C_{100} and C_{011} are proportional to Ω_L , while C_{200} , C_{111} , and C_{022} are on the scale of Ω_L^2 . By neglecting the higher orders of Ω_L in Eqs. (23), the amplitudes in the steady state are approximated as

$$C_{100} = -\frac{\Omega_L \kappa'}{\kappa'^2 - G^2}, \quad (24a)$$

$$C_{011} = \frac{G\Omega_L}{\kappa'^2 - G^2}, \quad (24b)$$

$$C_{200} = \frac{1}{\sqrt{2}} \frac{\Omega_L^2 (2\kappa'^2 - G^2)}{(\kappa'^2 - G^2)(2\kappa'^2 - 3G^2)}, \quad (24c)$$

$$C_{111} = -2 \frac{G\Omega_L^2 \kappa'}{(\kappa'^2 - G^2)(2\kappa'^2 - 3G^2)}, \quad (24d)$$

$$C_{022} = 2 \frac{G^2 \Omega_L^2}{(\kappa'^2 - G^2)(2\kappa'^2 - 3G^2)}. \quad (24e)$$

In the case of weak driving field, the probability of exciting one photon is larger than that of exciting two photons, $|C_{100}|^2 \gg |C_{200}|^2, |C_{111}|^2$. Thus, the second-order correlation function (20) is reduced to $g_{\text{ccw}}^{(2)}(0) \approx 2|C_{200}|^2/|C_{100}|^4$. Based on Eqs. (24), the approximate solution of the correlation function of the CCW mode is given by

$$g_{\text{ccw}}^{(2)}(0) = \frac{R(G)R(\frac{\sqrt{2}}{2}G)}{R(0)R(\frac{\sqrt{6}}{2}G)}, \quad (25)$$

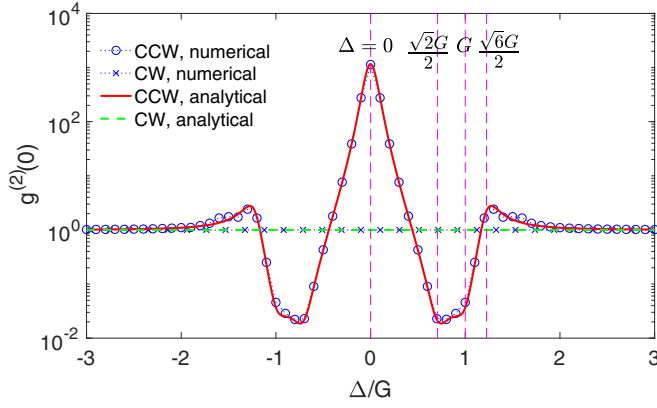


FIG. 3. Second-order correlation function $g^{(2)}(0)$ of CCW and CW modes versus Δ/G . Parameters are chosen as $G/\kappa = 10$, $\gamma/\kappa = 0.01$, $\Omega_L/\kappa = 0.1$, and $\bar{n}_{\text{th}} = 0$.

where $R(\omega) = [\kappa^2/4 + (\Delta - \omega)^2][\kappa^2/4 + (\Delta + \omega)^2]$. Using the expressions of the factors $R(\omega)$, we have the maximal values of $g_{\text{CCW}}^{(2)}(0)$ at $\Delta = 0, \pm\sqrt{6}G/2$, where the correlation function $g_{\text{CCW}}^{(2)}(0) > 1$, which indicates photon bunching. The minimal values of $g_{\text{CCW}}^{(2)}(0)$ appear at $\Delta = \pm G, \pm\sqrt{2}G/2$. At these positions, the correlation function $g_{\text{CCW}}^{(2)}(0) < 1$ denotes photon antibunching, where the probability of exciting the single-photon state in the CCW mode is higher than that of preparing a two-photon state.

Since the coupling between the CW mode and the Kittel mode is absent, the correlation function of the CW mode can be obtained by setting $G = 0$ in Eq. (25), and we have

$$g_{\text{CW}}^{(2)}(0) = 1. \quad (26)$$

Neither photon bunching nor photon antibunching happens for the CW mode.

Second-order correlation functions $g^{(2)}(0)$ of the CCW and CW modes as a function of Δ/G are plotted in Fig. 3. The analytical results (25) and (26) agree well with the numerical results based on the master equation (17). The correlation function $g_{\text{CCW}}^{(2)}(0)$ shows several peaks and dips, which originate from the nonlinear coupling between the CCW mode and the Kittel mode, while the correlation function for the CW mode is located at $g_{\text{CW}}^{(2)}(0) = 1$, as expected. The photon blockade $g_{\text{CCW}}^{(2)}(0) \ll 1$ at detuning $\Delta = \pm G$ comes from the single-photon transition $|0_0\rangle \rightarrow |1_{\pm}\rangle$. When the energy level splitting in single-photon subspace is larger than the cavity linewidth, i.e., $G > \kappa$, the single-photon transition can be spectrally resolved, but the subsequent transition $|1_{\pm}\rangle \rightarrow |2_0\rangle, |2_{\pm}\rangle$ is blocked for a large detuning, leading to photon blockade. The photon blockade occurs at $\Delta = \pm\sqrt{2}G/2$ and is due to destructive interference which suppresses the population in $|200\rangle$, as discussed in the two-mode optomechanical system [67]. The photon bunching at $\Delta = 0$ also comes from the destructive interference at $|100\rangle$, where the system is driven into a dark state $|\text{dark}\rangle \propto G|000\rangle - \Omega_L|011\rangle$, then couples to $|200\rangle$ via $|111\rangle$. At detuning $\Delta = \pm\sqrt{6}G/2$, the two-photon resonance transition $|0_0\rangle \rightarrow |2_{\pm}\rangle$ leads to the photon bunching $g_{\text{CCW}}^{(2)}(0) > 1$.

The correlation function $g_{\text{CCW}}^{(2)}(0)$ of the CCW mode as a function of G/κ is shown in Fig. 4. The correlation function decreases with the increasing of G/κ , and the strong-

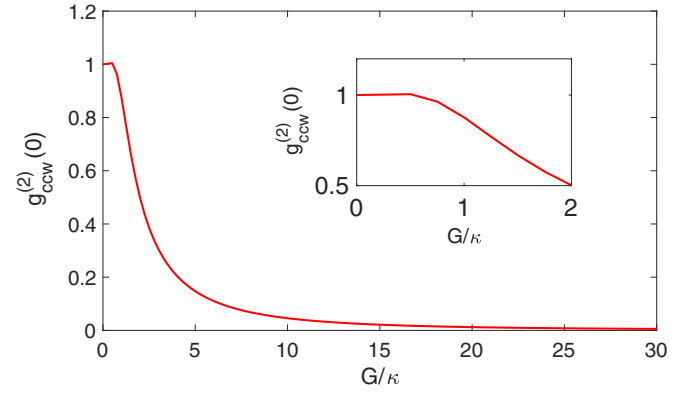


FIG. 4. Second-order correlation function $g_{\text{CCW}}^{(2)}(0)$ of the CCW mode as a function of G/κ at $\Delta = G$. Parameters are the same as in Fig. 3.

coupling condition $G > \kappa$ is necessary to realize photon blockade. In the weak-coupling regime, the transition $|0_0\rangle \rightarrow |1_{\pm}\rangle$ cannot be spectrally resolved, which hinders the realization of photon antibunching, as shown in the inset of Fig. 4.

Figure 5 displays the correlation function $g_{\text{CCW}}^{(2)}(0)$ of the CCW mode versus Δ/G for different values of \bar{n}_{th} . The qualities of photon bunching and antibunching are degraded with the increasing of \bar{n}_{th} , but both bunching and antibunching still survive for small thermal magnon occupations. For a YIG sphere with magnon frequency $\omega_m = 7.95$ GHz, the average thermal magnon number in a dilution refrigerator at temperature 10 mK is $n_0 = 0.026$ [68]. The small thermal magnon occupations little affect the photon statistical properties. Figure 5 also shows several new resonances emerge in the correlation function which are absent for $\bar{n}_{\text{th}} = 0$. To understand these new features, we assumed that the magnon mode is initially in a thermal state and the cavity is in a vacuum, and the system can be described by the density matrix $\rho = (1 - p) \sum_{m_k \geq 0} p^{m_k} |00m_k\rangle\langle 00m_k|$, where $p = \exp(-\hbar\omega_m/k_B T)$. In this case, the splitting of the energy level in the one- and two-photon subspaces is m_k dependent, the individual resonances within each m_k subspace start to overlap, and the cumulative

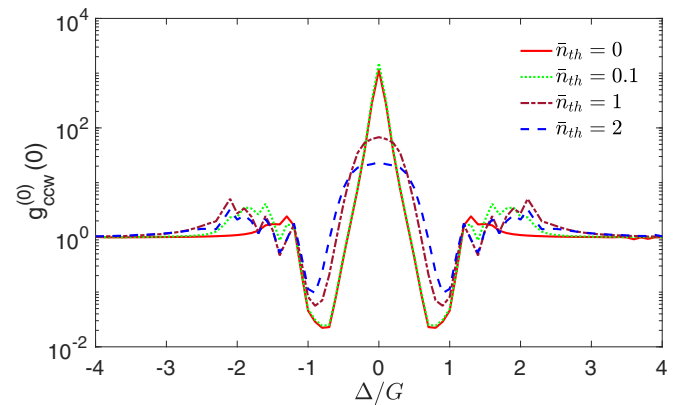


FIG. 5. Second-order correlation function $g_{\text{CCW}}^{(2)}(0)$ of the CCW mode as a function of Δ/G for different values of \bar{n}_{th} . Parameters are the same as in Fig. 3.

effect of different magnon numbers leads to the new bunching and antibunching features [67,69].

IV. DISCUSSION AND CONCLUSIONS

By studying the second-order correlation function, we found that the single-photon-magnon strong coupling $G > \kappa$ is required to realize the photon blockade. In current YIG-based experiments, the measured values of G are still significantly smaller than the cavity damping rate κ . Great efforts have been made to enhance optomagnonic coupling; it was shown that the coupling strength can be enhanced by reducing the mode volume of the optical mode [22,33,34], selecting magnon modes to maximize the overlap of the magnon and photon modes [25], or designing an optomagnonic crystal [65]. Besides the YIG crystal, new magnetic materials could also be investigated for optomagnonics. Recent studies predicted that in magnetized epsilon-near-zero media the single-photon-magnon coupling strength can be enhanced close to the magnon frequency in the gigahertz range [70,71]. Although current experiments are still far away from the required coupling strength, it is to be expected that the coupling strength can be improved in the future. Moreover, the unconventional photon blockade which

utilizes the destructive interference in the two-photon excitation state needs only weakly nonlinear coupling [54–56]. The extension of our scheme to the unconventional photon blockade can relax the requirement of the strong-coupling condition.

In summary, we have studied nonreciprocal photon blockade in a cavity optomagnonics system. Due to the selection rules of angular momentum and the triple-resonance condition, the system presents a nonreciprocal optomagnonic coupling, in which magnons couple to only one of the linearly polarized CCW or CW WGM photons. This enables the realization of nonreciprocal photon blockade in the single-photon-magnon strong-coupling regime. Our proposal suggests that a cavity optomagnonics system may be an attractive platform for studying chiral quantum optics. In addition, it would be interesting if our study could be extended to chiral metamaterials [72–76] for applications of nonreciprocal devices.

ACKNOWLEDGMENTS

We acknowledge support from the National Natural Science Foundation of China (Grants No. 12174054, No. 12074067, and No. 11847056) and the Natural Science Foundation of Fujian Province of China (Grants No. 2021J011228 and No. 2020J01191).

-
- [1] P. Lodahl, S. Mahmoodian, S. Stobbe, A. Rauschenbeutel, P. Schneeweiss, J. Volz, H. Pichler, and P. Zoller, Chiral quantum optics, *Nature (London)* **541**, 473 (2017).
 - [2] D. L. Sounas and A. Alù, Non-reciprocal photonics based on time modulation, *Nat. Photonics* **11**, 774 (2017).
 - [3] L. Fan, J. Wang, L. T. Varghese, H. Shen, B. Niu, Y. Xuan, A. M. Weiner, and M. Qi, An all-silicon passive optical diode, *Science* **335**, 447 (2012).
 - [4] Y. Shi, Z. Yu, and S. Fan, Limitations of nonlinear optical isolators due to dynamic reciprocity, *Nat. Photonics* **9**, 388 (2015).
 - [5] J. Kim, M. C. Kuzyk, K. Han, H. Wang, and G. Bahl, Non-reciprocal Brillouin scattering induced transparency, *Nat. Phys.* **11**, 275 (2015).
 - [6] C.-H. Dong, Z. Shen, C.-L. Zou, Y.-L. Zhang, W. Fu, and G.-C. Guo, Brillouin-scattering-induced transparency and non-reciprocal light storage, *Nat. Commun.* **6**, 6193 (2015).
 - [7] Z. Shen, Y.-L. Zhang, Y. Chen, C.-L. Zou, Y.-F. Xiao, X.-B. Zou, F.-W. Sun, G.-C. Guo, and C.-H. Dong, Experimental realization of optomechanically induced non-reciprocity, *Nat. Photonics* **10**, 657 (2016).
 - [8] Q.-T. Cao, H. Wang, C.-H. Dong, H. Jing, R.-S. Liu, X. Chen, L. Ge, Q. Gong, and Y.-F. Xiao, Experimental Demonstration of Spontaneous Chirality in a Nonlinear Microresonator, *Phys. Rev. Lett.* **118**, 033901 (2017).
 - [9] E. Verhagen and A. Alù, Optomechanical nonreciprocity, *Nat. Phys.* **13**, 922 (2017).
 - [10] C. Caloz, A. Alù, S. Tretyakov, D. Sounas, K. Achouri, and Z.-L. Deck-Léger, Electromagnetic Nonreciprocity, *Phys. Rev. Appl.* **10**, 047001 (2018).
 - [11] A. Rosario Hamann, C. Müller, M. Jerger, M. Zanner, J. Combes, M. Pletyukhov, M. Weides, T. M. Stace, and A. Fedorov, Nonreciprocity Realized with Quantum Nonlinearity, *Phys. Rev. Lett.* **121**, 123601 (2018).
 - [12] E. A. Kittlaus, W. M. Jones, P. T. Rakich, N. T. Otterstrom, R. E. Muller, and M. Rais-Zadeh, Electrically driven acousto-optics and broadband non-reciprocity in silicon photonics, *Nat. Photonics* **15**, 43 (2021).
 - [13] S. Kim, D. B. Sohn, C. W. Peterson, and G. Bahl, On-chip optical non-reciprocity through a synthetic Hall effect for photons, *APL Photonics* **6**, 011301 (2021).
 - [14] H. Tian, J. Liu, A. Siddharth, R. N. Wang, T. Blésin, J. He, T. J. Kippenberg, and S. A. Bhave, Magnetic-free silicon nitride integrated optical isolator, *Nat. Photonics* **15**, 828 (2021).
 - [15] D. B. Sohn, O. E. Örsel, and G. Bahl, Electrically driven optical isolation through phonon-mediated photonic Autler–Townes splitting, *Nat. Photonics* **15**, 822 (2021).
 - [16] S. Mailis, On-chip non-magnetic optical isolator, *Nat. Photonics* **15**, 794 (2021).
 - [17] R. Hisatomi, A. Osada, Y. Tabuchi, T. Ishikawa, A. Noguchi, R. Yamazaki, K. Usami, and Y. Nakamura, Bidirectional conversion between microwave and light via ferromagnetic magnons, *Phys. Rev. B* **93**, 174427 (2016).
 - [18] X. Zhang, N. Zhu, C.-L. Zou, and H. X. Tang, Optomagnonic Whispering Gallery Microresonators, *Phys. Rev. Lett.* **117**, 123605 (2016).
 - [19] J. A. Haigh, A. Nunnenkamp, A. J. Ramsay, and A. J. Ferguson, Triple-Resonant Brillouin Light Scattering in Magneto-optical Cavities, *Phys. Rev. Lett.* **117**, 133602 (2016).
 - [20] T. Liu, X. Zhang, H. X. Tang, and M. E. Flatté, Optomagnonics in magnetic solids, *Phys. Rev. B* **94**, 060405(R) (2016).

- [21] S. Viola Kusminskiy, H. X. Tang, and F. Marquardt, Coupled spin-light dynamics in cavity optomagnonics, *Phys. Rev. A* **94**, 033821 (2016).
- [22] J. Graf, H. Pfeifer, F. Marquardt, and S. Viola Kusminskiy, Cavity optomagnonics with magnetic textures: Coupling a magnetic vortex to light, *Phys. Rev. B* **98**, 241406(R) (2018).
- [23] J. A. Haigh, N. J. Lambert, S. Sharma, Y. M. Blanter, G. E. W. Bauer, and A. J. Ramsay, Selection rules for cavity-enhanced Brillouin light scattering from magnetostatic modes, *Phys. Rev. B* **97**, 214423 (2018).
- [24] S. Sharma, Y. M. Blanter, and G. E. W. Bauer, Optical Cooling of Magnons, *Phys. Rev. Lett.* **121**, 087205 (2018).
- [25] S. Sharma, B. Z. Rameshti, Y. M. Blanter, and G. E. W. Bauer, Optimal mode matching in cavity optomagnonics, *Phys. Rev. B* **99**, 214423 (2019).
- [26] V. A. S. V. Bittencourt, V. Feulner, and S. Viola Kusminskiy, Magnon heralding in cavity optomagnonics, *Phys. Rev. A* **100**, 013810 (2019).
- [27] W.-J. Wu, Y.-P. Wang, J.-Z. Wu, J. Li, and J. Q. You, Remote magnon entanglement between two massive ferrimagnetic spheres via cavity optomagnonics, *Phys. Rev. A* **104**, 023711 (2021).
- [28] R. Hisatomi, A. Noguchi, R. Yamazaki, Y. Nakata, A. Gloppe, Y. Nakamura, and K. Usami, Helicity-Changing Brillouin Light Scattering by Magnons in a Ferromagnetic Crystal, *Phys. Rev. Lett.* **123**, 207401 (2019).
- [29] S. Sharma, V. A. S. V. Bittencourt, A. D. Karenowska, and S. Viola Kusminskiy, Spin cat states in ferromagnetic insulators, *Phys. Rev. B* **103**, L100403 (2021).
- [30] F.-X. Sun, S.-S. Zheng, Y. Xiao, Q. Gong, Q. He, and K. Xia, Remote Generation of Magnon Schrödinger Cat State Via Magnon-Photon Entanglement, *Phys. Rev. Lett.* **127**, 087203 (2021).
- [31] F. Šimić, S. Sharma, Y. M. Blanter, and G. E. W. Bauer, Coherent pumping of high-momentum magnons by light, *Phys. Rev. B* **101**, 100401(R) (2020).
- [32] D. Lachance-Quirion, Y. Tabuchi, A. Gloppe, K. Usami, and Y. Nakamura, Hybrid quantum systems based on magnonics, *Appl. Phys. Express* **12**, 070101 (2019).
- [33] J. A. Haigh, R. A. Chakalov, and A. J. Ramsay, Subpicoliter Magnetooptical Cavities, *Phys. Rev. Appl.* **14**, 044005 (2020).
- [34] N. Zhu, X. Zhang, X. Han, C.-L. Zou, C. Zhong, C.-H. Wang, L. Jiang, and H. X. Tang, Waveguide cavity optomagnonics for microwave-to-optics conversion, *Optica* **7**, 1291 (2020).
- [35] H. Xie, Z.-G. Shi, L.-W. He, X. Chen, C.-G. Liao, and X.-M. Lin, Proposal for a Bell test in cavity optomagnonics, *Phys. Rev. A* **105**, 023701 (2022).
- [36] S. Viola Kusminskiy, Cavity optomagnonics, in *Optomagnonic Structures: Novel Architectures for Simultaneous Control of Light and Spin Waves* (World Scientific, Singapore, 2021), pp. 299–353.
- [37] B. Zare Rameshti, S. Viola Kusminskiy, J. A. Haigh, K. Usami, D. Lachance-Quirion, Y. Nakamura, C.-M. Hu, H. X. Tang, G. E. Bauer, and Y. M. Blanter, Cavity magnonics, *Phys. Rep.* **979**, 1 (2022).
- [38] J. A. Haigh, A. Nunnenkamp, and A. J. Ramsay, Polarization Dependent Scattering in Cavity Optomagnonics, *Phys. Rev. Lett.* **127**, 143601 (2021).
- [39] H. Yuan, Y. Cao, A. Kamra, R. A. Duine, and P. Yan, Quantum magnonics: When magnon spintronics meets quantum information science, *Phys. Rep.* **965**, 1 (2022).
- [40] L. M. Sandratskii and P. Buczek, Lifetimes and chirality of spin waves in antiferromagnetic and ferromagnetic FeRh from the perspective of time-dependent density functional theory, *Phys. Rev. B* **85**, 020406(R) (2012).
- [41] Y.-P. Wang, J. W. Rao, Y. Yang, P.-C. Xu, Y. S. Gui, B. M. Yao, J. Q. You, and C. M. Hu, Nonreciprocity and Unidirectional Invisibility in Cavity Magnonics, *Phys. Rev. Lett.* **123**, 127202 (2019).
- [42] N. Zhu, X. Han, C.-L. Zou, M. Xu, and H. X. Tang, Magnon-photon strong coupling for tunable microwave circulators, *Phys. Rev. A* **101**, 043842 (2020).
- [43] X. Zhang, A. Galda, X. Han, D. Jin, and V. M. Vinokur, Broadband Nonreciprocity Enabled by Strong Coupling of Magnons and Microwave Photons, *Phys. Rev. Appl.* **13**, 044039 (2020).
- [44] C. Zhao, R. Peng, Z. Yang, S. Chao, C. Li, Z. Wang, and L. Zhou, Nonreciprocal amplification in a cavity magnonics system, *Phys. Rev. A* **105**, 023709 (2022).
- [45] S. Sharma, Y. M. Blanter, and G. E. W. Bauer, Light scattering by magnons in whispering gallery mode cavities, *Phys. Rev. B* **96**, 094412 (2017).
- [46] A. Osada, A. Gloppe, Y. Nakamura, and K. Usami, Orbital angular momentum conservation in Brillouin light scattering within a ferromagnetic sphere, *New J. Phys.* **20**, 103018 (2018).
- [47] Y.-L. Ren, S.-L. Ma, J.-K. Xie, X.-K. Li, and F.-L. Li, Nonreciprocal optical transmission in cavity optomagnonics, *Opt. Express* **29**, 41399 (2021).
- [48] A. Osada, R. Hisatomi, A. Noguchi, Y. Tabuchi, R. Yamazaki, K. Usami, M. Sadgrove, R. Yalla, M. Nomura, and Y. Nakamura, Cavity Optomagnonics with Spin-Orbit Coupled Photons, *Phys. Rev. Lett.* **116**, 223601 (2016).
- [49] A. Osada, A. Gloppe, R. Hisatomi, A. Noguchi, R. Yamazaki, M. Nomura, Y. Nakamura, and K. Usami, Brillouin Light Scattering by Magnetic Quasivortices in Cavity Optomagnonics, *Phys. Rev. Lett.* **120**, 133602 (2018).
- [50] R. Huang, A. Miranowicz, J.-Q. Liao, F. Nori, and H. Jing, Nonreciprocal Photon Blockade, *Phys. Rev. Lett.* **121**, 153601 (2018).
- [51] A. Imamoglu, H. Schmidt, G. Woods, and M. Deutsch, Strongly Interacting Photons in a Nonlinear Cavity, *Phys. Rev. Lett.* **79**, 1467 (1997).
- [52] K. M. Birnbaum, A. Boca, R. Miller, A. D. Boozer, T. E. Northup, and H. J. Kimble, Photon blockade in an optical cavity with one trapped atom, *Nature (London)* **436**, 87 (2005).
- [53] K. Müller, A. Rundquist, K. A. Fischer, T. Sarmiento, K. G. Lagoudakis, Y. A. Kelaita, C. Sánchez Muñoz, E. del Valle, F. P. Laussy, and J. Vučković, Coherent Generation of Nonclassical Light on Chip via Detuned Photon Blockade, *Phys. Rev. Lett.* **114**, 233601 (2015).
- [54] T. C. H. Liew and V. Savona, Single Photons from Coupled Quantum Modes, *Phys. Rev. Lett.* **104**, 183601 (2010).
- [55] H. Flayac and V. Savona, Unconventional photon blockade, *Phys. Rev. A* **96**, 053810 (2017).
- [56] H. J. Snijders, J. A. Frey, J. Norman, H. Flayac, V. Savona, A. C. Gossard, J. E. Bowers, M. P. van Exter, D. Bouwmeester, and W. Löffler, Observation of the Unconventional Photon Blockade, *Phys. Rev. Lett.* **121**, 043601 (2018).

- [57] B. Li, R. Huang, X. Xu, A. Miranowicz, and H. Jing, Nonreciprocal unconventional photon blockade in a spinning optomechanical system, *Photonics Res.* **7**, 630 (2019).
- [58] H. Z. Shen, Q. Wang, J. Wang, and X. X. Yi, Nonreciprocal unconventional photon blockade in a driven dissipative cavity with parametric amplification, *Phys. Rev. A* **101**, 013826 (2020).
- [59] W. Xue, H. Shen, and X. Yi, Nonreciprocal conventional photon blockade in driven dissipative atom-cavity, *Opt. Lett.* **45**, 4424 (2020).
- [60] Y.-W. Jing, H.-Q. Shi, and X.-W. Xu, Nonreciprocal photon blockade and directional amplification in a spinning resonator coupled to a two-level atom, *Phys. Rev. A* **104**, 033707 (2021).
- [61] J. Wang, Q. Wang, and H. Shen, Nonreciprocal unconventional photon blockade with spinning atom-cavity, *Europhys. Lett.* **134**, 64003 (2021).
- [62] X. Xu, Y. Zhao, H. Wang, H. Jing, and A. Chen, Quantum nonreciprocity in quadratic optomechanics, *Photonics Res.* **8**, 143 (2020).
- [63] X.-W. Xu, Y. Li, B. Li, H. Jing, and A.-X. Chen, Nonreciprocity via Nonlinearity and Synthetic Magnetism, *Phys. Rev. Appl.* **13**, 044070 (2020).
- [64] H. Le Gall, T. K. Vien, and B. Desormiere, Theory of the elastic and inelastic scattering of light by magnetic crystals. II. Second-order processes, *Phys. Status Solidi B* **47**, 591 (1971).
- [65] J. Graf, S. Sharma, H. Huebl, and S. V. Kusminskiy, Design of an optomagnonic crystal: Towards optimal magnon-photon mode matching at the microscale, *Phys. Rev. Res.* **3**, 013277 (2021).
- [66] G. Schunk, J. U. Furst, M. Fortsch, D. V. Strekalov, U. Vogl, F. Sedlmeir, H. G. Schwefel, G. Leuchs, and C. Marquardt, Identifying modes of large whispering-gallery mode resonators from the spectrum and emission pattern, *Opt. Express* **22**, 30795 (2014).
- [67] P. Komar, S. D. Bennett, K. Stannigel, S. J. M. Habraken, P. Rabl, P. Zoller, and M. D. Lukin, Single-photon nonlinearities in two-mode optomechanics, *Phys. Rev. A* **87**, 013839 (2013).
- [68] D. Lachance-Quirion, Y. Tabuchi, S. Ishino, A. Noguchi, T. Ishikawa, R. Yamazaki, and Y. Nakamura, Resolving quanta of collective spin excitations in a millimeter-sized ferromagnet, *Sci. Adv.* **3**, e1603150 (2017).
- [69] H. Xie, G.-W. Lin, X. Chen, Z.-H. Chen, and X.-M. Lin, Single-photon nonlinearities in a strongly driven optomechanical system with quadratic coupling, *Phys. Rev. A* **93**, 063860 (2016).
- [70] V. A. S. V. Bittencourt, I. Liberal, and S. Viola Kusminskiy, Optomagnonics in Dispersive Media: Magnon-Photon Coupling Enhancement at the Epsilon-Near-Zero Frequency, *Phys. Rev. Lett.* **128**, 183603 (2022).
- [71] V. A. S. V. Bittencourt, I. Liberal, and S. Viola Kusminskiy, Light propagation and magnon-photon coupling in optically dispersive magnetic media, *Phys. Rev. B* **105**, 014409 (2022).
- [72] L. Ouyang, W. Wang, D. Rosenmann, D. A. Czaplewski, J. Gao, and X. Yang, Near-infrared chiral plasmonic metasurface absorbers, *Opt. Express* **26**, 31484 (2018).
- [73] M. S. Mahmud, D. Rosenmann, D. A. Czaplewski, J. Gao, and X. Yang, Plasmon-phonon coupling between mid-infrared chiral metasurfaces and molecular vibrations, *Opt. Express* **28**, 21192 (2020).
- [74] H. Tang, D. Rosenmann, D. A. Czaplewski, X. Yang, and J. Gao, Dual-band selective circular dichroism in mid-infrared chiral metasurfaces, *Opt. Express* **30**, 20063 (2022).
- [75] A. Dasgupta, J. Gao, and X. Yang, Atomically thin nonlinear transition metal dichalcogenide holograms, *Nano Lett.* **19**, 6511 (2019).
- [76] A. Dasgupta, X. Yang, and J. Gao, Nonlinear beam shaping with binary phase modulation on patterned WS₂ monolayer, *ACS Photonics* **7**, 2506 (2020).